ELSEVIER

Earth and Planetary Science Letters 5836 (2001) 1–17

EPSL

www.elsevier.com/locate/epsl

A new approach to stable isotope-based paleoaltimetry: implications for paleoaltimetry and paleohypsometry of the High Himalaya since the Late Miocene

David B. Rowley *, Raymond T. Pierrehumbert, Brian S. Currie [1]

Department of the Geophysical Sciences, 5734 S. Ellis Avenue, The University of Chicago, Chicago, IL 60637, USA

Received 17 July 2000; received in revised form 14 March 2001; accepted 14 March 2001

Abstract

The change in oxygen isotopic composition of precipitation is modeled using equilibrium fractionation during Rayleigh distillation linked to the thermodynamics of atmospheric ascent and water vapor condensation. The primary controllers of the vertical variation in isotopic composition with elevation are the low elevation temperature and relative humidity as these control the vertical distribution of condensation. An empirical fit of precipitation versus model condensation based on Alpine stations is derived. This fit is represented in the model as the weighted mean composition of condensation within a 1000 m thick air parcel 1500 ± 500 m above the ground surface and is used for all other regions. Comparison of model versus observed modern precipitation reveals a close fit, particularly of more highly elevated sites. Comparison of modern waters in the Himalayas and southern Tibet with model predictions, particularly as revealed by comparison of observed and predicted hypsometry provides additional support to the validity of the model. Finally, application of this model to estimates of paleo-waters in the Himalayas and southern Tibet reveals that this region had already achieved its present hypsometry by the Late Miocene, about 10 Ma ago. © 2001 Published by Elsevier Science B.V.

Keywords: paleoaltimetry; paleohypsometry; oxygen isotopes; Himalayas; Tibet

1. Introduction

The distribution of surface elevations provides first-order information on crustal, lithospheric and upper mantle dynamics [1,2]. The general, but, by no means universal correlation of topography and crustal thickness has long been employed to discern regions effected by crustal thickening and thinning. More recently mantle contributions to surface topography have been increasingly understood and promoted as explanations of both anomalously high (e.g. Africa) [3] and low continents (e.g. Australia), anomalous depths of back arc basins [4,5], and offered as a mechanism by which Tibet might have risen by perhaps 2 km within the past 5–10 million years [1]. In addition, topography significantly influences Earth's climate, particularly the distribution of precipitation as well as aspects of the large scale

* Corresponding author. Tel.: +1-1773-702-4071; Fax: +1-1773-702-9505; E-mail: rowley@plates.uchicago.edu

[1] Present address: Department of Geology, 125 Shidler Hall, Miami University, Oxford, OH 45056, USA.

0012-821X/01/$ – see front matter © 2001 Published by Elsevier Science B.V.
PII: S0012-821X(01)00324-7

circulation [6–9], including the Asian monsoon [8,10]. Earth scientists have a first-order understanding of why the modern distribution of topography exists and through inferences based on geologic history guesses have been made as to its historical development. However, there are virtually no means of quantitatively determining how high a given region has been at any time in the past and thus of testing any of the models that have been proposed to explain the distribution. Chase et al. [11] and Forest et al. [12] review the problem and highlight existing qualitative and quantitative approaches.

In this paper we provide the theoretical basis for a method that employs the stable isotopes of oxygen and hydrogen for paleoaltimetry and paleohypsometry and an assessment of the uncertainties of the method. We then apply this new method to some recently obtained data from the Late Miocene to Plio–Pleistocene carbonate-bearing sediments from the High Himalayas in order to estimate the heights of this region since about 8 million years [13].

2. Modeling oxygen and hydrogen isotopes in precipitation

In order to provide independent estimates of paleoaltitude, we make use of a simple model that describes the systematic behavior of the isotopes of oxygen in precipitation as a function of elevation. The model is equally well employed with the stable isotopes of hydrogen, but for the sake of brevity here we simply discuss oxygen. The present discussion extends the model used to interpret the isotopic composition of Last Glacial Maximum age ice in the Andes [14]. We compare predictions of model oxygen isotopic compositions with long-term precipitation records from the Swiss Alps in order to establish viability of the general model and to determine a reasonable scheme for sampling condensation at altitude and converting it into precipitation falling onto a surface at a specific elevation. We then compare modern $\delta^{18}O$ isotopic compositions of low latitude (0° to ±35°) International Atomic Energy Agency–Global Network of Isotopes in Precipitation (IAEA–GNIP) stations with predictions and demonstrate the close correlation between observation and model results.

This work is significantly different from the recent applications of isotopes to paleoaltimetry by Drummond et al. [15], Chamberlain and Poage [16] and Garzione et al. [17] that employ either 'global' or local empirical linear calibrations of the isotopic lapse rates of precipitation and or surface waters. In this study the underlying thermodynamics of both isotopes and atmospheric condensation are used to understand why and what the important controls are on the isotopic lapse rate. This then allows direct assessment of how changes in climate parameters might affect the result and what limitations might exist for application in different climatic situations.

The oxygen and hydrogen isotopic composition of precipitation has long been a research focus of meteorologists and geochemists. Analyses of the IAEA–GNIP data sets have revealed that a number of factors, including temperature, monthly precipitation, latitude, continentality, and altitude contribute to the isotopic composition of precipitation [18–21]. For our purposes, the important conclusion derived from these analyses is that Rayleigh-type fractionation models adequately account for the isotopic composition of precipitation, and underlie physical explanations of the various effects identified in past studies (e.g. [18,20]).

Various models have been discussed in the literature that describe the spatial distribution of isotopes in precipitation, ranging from one-dimensional to atmospheric general circulation models (e.g. [18,22–27]). Below we outline a simple parcel-based model that tracks the moist static energy, water vapor content and water vapor isotopic composition along ascending, precipitating trajectories.

3. The model

At equilibrium, the fractionation of ^{18}O relative to ^{16}O and D relative to H, between precipitation and water vapor is determined by the fractiona-

tion factor α, which for oxygen is defined as:

$$\alpha_O = R_p/R_v = (\delta^{18}O_p + 1000)/(\delta^{18}O_v + 1000)$$

where R_p and R_v are the ratio of $^{18}O/^{16}O$ in precipitation and water vapor, respectively. The quantities $\delta^{18}O_p$, $\delta^{18}O_v$ are the ratios in precipitation and vapor, respectively, relative to a standard, (SMOW) expressed as per mil, such that, for oxygen:

$$\delta^{18}O_p = (R_p/R_{SMOW} - 1)\ 1000$$

Identical relations exist for D/H fractionation. The fractionation factor, α, is a function of the temperature at which fractionation takes place and the phases involved. In the atmosphere, fractionation occurs between water vapor and liquid water or between water vapor and water ice. The temperature dependence of $\alpha(T)$ has been determined experimentally for liquid–vapor equilibrium [28,29], and for ice–vapor equilibrium [30]. Existing experimental results are in very close agreement and we use the relations, for oxygen:

$$1000\ \ln\alpha_O(T)_{l-v} = -7.685 + 6.7123\ (10^3T^{-1}) - 1.6664(10^6T^{-2}) + 0.35041(10^9T^{-3})$$

$$1000\ \ln\alpha_O(T)_{i-v} = 11839/T - 28.224$$

where T is the temperature in Kelvin and α_O with subscripts l, v, and i are liquid, vapor, and ice, respectively. Because liquid water can be cooled below the freezing temperature of water by 20 K or more there is not an abrupt step in α_O at 273.15 K. Thus for temperatures between 273.15 K and 253.15 K we blend between ice and liquid water fractionation. At any given T the equilibrium isotopic compositions of oxygen, for example, in precipitate ($\delta^{18}O_p$) and vapor ($\delta^{18}O_v$) are described by the relation:

$$\delta^{18}O_p = \alpha_O(T)(\delta^{18}O_v + 1000) - 1000.$$

Rayleigh condensation treats the isotopic composition as an open system distillation in which precipitation is successively removed as it condenses from the vapor leaving the residual vapor progressively depleted in ^{18}O. We use $\zeta = -\ln(p/p_s)$ as our vertical coordinate, where p is ambient pressure and p_s is the surface pressure. The distillation process can then be expressed by the differential equation:

$$\frac{dR_v}{d\zeta} = \frac{dR_p}{d\zeta} = R_v\ (\alpha(T) - 1)\frac{1}{q}\frac{dq}{d\zeta} \quad (1)$$

where R_p and R_v are the ratios in the incremental precipitation and vapor, respectively, q is the mass mixing ratio of water, and $dq/d\zeta$ is the amount of water condensed from the air parcel in order to maintain saturation associated with adiabatic ascent. From atmospheric thermodynamics it is possible to determine $dq/d\zeta$ with three basic equations. These are:

$$\frac{dz}{d\zeta} = \frac{RT}{g} \quad (2)$$

where z is altitude in m, and R (without any subscripts) is the gas constant for air. The change in temperature with height depends on whether or not condensation is occurring, and for rapidly ascending, thermally isolated parcels is described by the relations:

$$\frac{dT}{d\zeta} = -\frac{RT + Lq_s}{C_p + Lq_s(\ln(e_s))'} \quad \text{if moisture is condensing} \quad (3a)$$

$$\frac{dT}{d\zeta} = -(R/C_p)\ T \quad \text{if non-condensing } (q < q_s) \quad (3b)$$

where C_p is the heat capacity of air, q_s is the saturation mass mixing ratio of water ($\approx 0.622\ e_s/p$), e_s is $e_s(T)$, which is the saturation vapor pressure of water as a function of T, and L is the latent heat contribution due to condensation, which also varies as a function of T. Eq. 3b is the formula for the dry adiabat. Eq. 3a incorporates the change in saturation vapor pressure with tem-

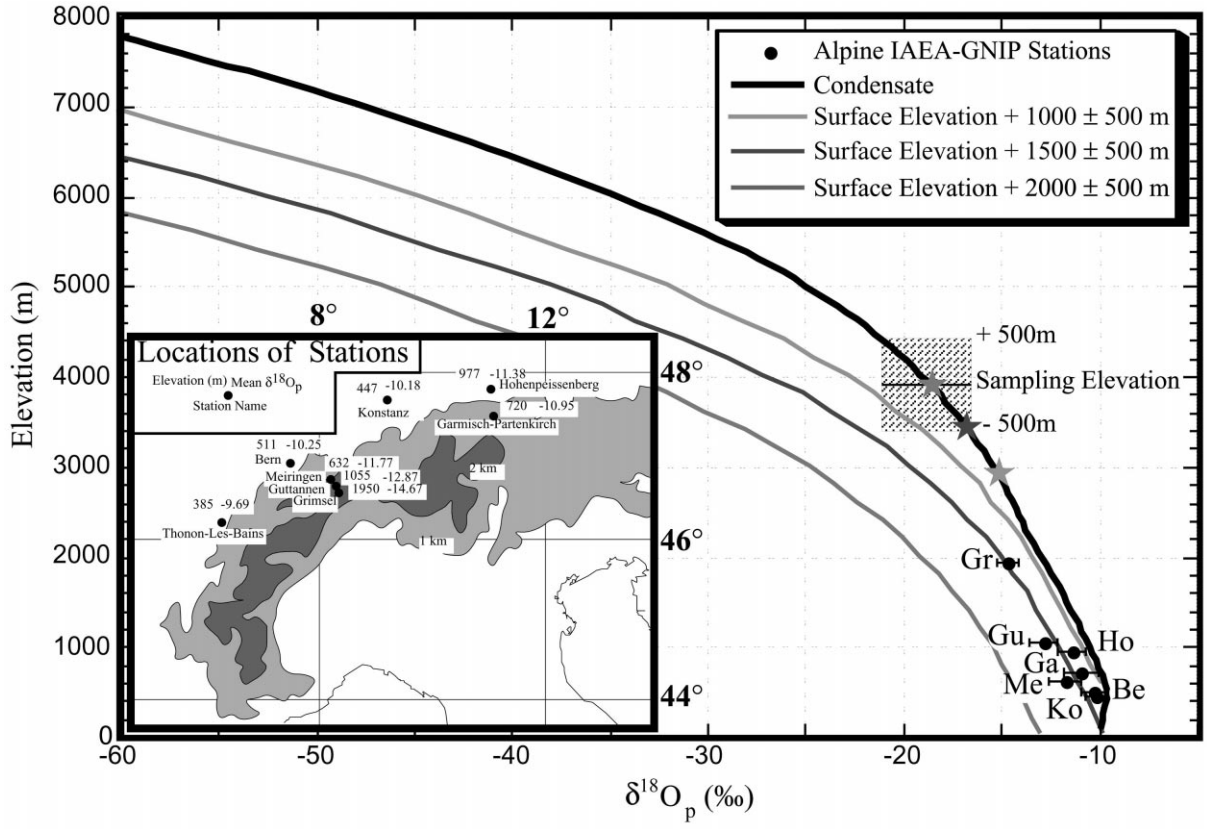

Fig. 1. Trajectories of the isotopic composition of vapor-derived condensate (black) and weighted mean $\delta^{18}O_p$ derived from 1000 m (light gray), 1500 m (dark gray), and 2000 m (medium gray) above the ground surface sampled within a layer 1000 m thick. The vapor-derived condensate trajectory is based on a RH of 80% at low elevations and starting T of 287 K. This RH is based on long-term means from the NCEP reanalysis project [31]. The starting value of $\delta^{18}O_v$ was chosen to yield precipitation compatible with the low elevation stations. Box with dashes represents the sampling interval with the stars gray-scale coordinated with the curves to represent the mean heights from which precipitation would be derived for each of the three curves for the station corresponding to Grimsel. Weighted mean annual isotopic compositions and reported 1σ standard deviations of IAEA stations (dots with error bars) [33] plotted at each station's elevation compared with model-derived weighted mean precipitation for the Alps. Inset map: Locations of IAEA stations and their heights and weighted mean $\delta^{18}O_p$ as reported by [33]. Abbreviations: Ko, Konstanz; Be, Bern; Me, Meiringen; Ga, Garmisch-Pertenkirch; Gu, Guttannen; Gr, Garmisch. Note that Meiringen and Guttannen are located deep within the Alps in the Aare valley and hence precipitation falling there is likely more fractionated than typical of their station elevations.

perature through the expression:

$$(\ln(e_s))' = \frac{1}{e_s}\frac{de_s}{dT}$$

Finally, the amount of water condensed from the air parcel as ice or liquid in order to maintain saturation is determined through the relation:

$$\frac{1}{q}\frac{dq}{d\zeta} = 1 + (\ln(e_s))' \quad \frac{dT}{d\zeta} \quad \text{if condensing } (q \geq q_s) \tag{4a}$$

$$\frac{1}{q}\frac{dq}{d\zeta} = 0 \quad \text{if non} - \text{condensing } (q < q_s) \tag{4b}$$

If there is no condensation, q is conserved following the air parcel.

In order to compute the vertical variation of the absolute value of $\delta^{18}O_p$, the boundary conditions that need to be specified are T, relative humidity (RH), and $\delta^{18}O_v$ at low elevation before orographic ascent. With these parameters specified the model then computes the thermodynamic equilibrium relationship for the parcel of air as it ascends. Air starting at the ground is lifted using (Eq. 3b) and (Eq. 4b) until $q = q_s$, whereafter condensation starts and Eq. 3a and Eq. 4a are used. Fig. 1 shows the trajectory of predicted composition of precipitation with altitude for a particular combination of T, RH, and $\delta^{18}O_v$.

In order to portray the composition of model precipitation at the ground surface rather than at the site of condensation we show three curves that sample the condensate from within a parcel of 1000 m thickness centered at elevations of 1000, 1500 and 2000 m above the surface. These three curves reflect the weighted mean of the isotopic composition of the precipitate, where the weights are based on $1/q\ dq/dz$. The best fit to the compositions observed at Alpine stations (Fig. 1) is provided by the model in which the precipitation reaching the ground is derived from a mean altitude of 1500 m above the surface. A comparison (not shown) between the slopes of observation and model compositions versus elevation over appropriate elevation ranges are indistinguishable. We employ this scheme for modeling the isotopic composition of precipitation in all other regions.

The model is mathematically one-dimensional, in that the equations need only be integrated with respect to ζ. However, the trajectories themselves can wander horizontally in an arbitrarily complex way as the parcel ascends. The chief physical assumption is that the air parcel remains relatively isolated from the surrounding air. Note that in our case, the model only needs to be valid for trajectories that produce precipitation. It need not reproduce the observed temperature and moisture profiles everywhere.

The isotopic composition of the vapor before orographic ascent is one of the boundary conditions needed as input to the model. We do not in general know this value and thus this introduces potential uncertainty. However, we are really interested in the difference in isotopic composition

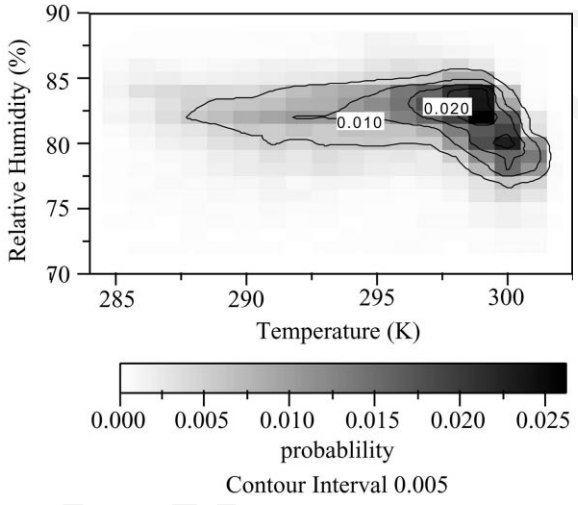

Fig. 2. Probability distribution function of T and RH extracted over entirely oceanic areas of the low latitude ($<35°$) part of the Earth from the 40 year NCEP-CDAS reanalysis output [31]. Mean $T = 295.5\ K \pm 4.1$ and mean $RH = 80.2\% \pm 3.9$ of the model and of the modern low latitude sea level ocean distribution. Sampling of T and RH from within this distribution provides an estimate of the variance of resulting isotopic compositions as a function of elevation as modeled in Fig. 3.

of precipitation falling at low elevation (essentially sea level) and higher elevation, as it is this difference, rather than the actual isotopic composition that correlates with altitude. Thus if we have two coeval sites, one at low elevation and a nearby potentially elevated site, it is the difference in their isotopic compositions that is referred to as $\Delta(\delta^{18}O_p)$ following [19] that correlates with the (paleo)altitude of the second site.

Uncertainties derive from (1) the variability of input parameters, specifically T and RH to which the model is quite sensitive, (2) evaporation and exchange [18] as the precipitation falls, and (3) turbulent mixing within the clouds during ascent. Temperature and RH are not arbitrarily variable on Earth. Thus uncertainty resulting from T and RH are limited by the variability of these parameters. As a starting point we focus on low latitude ($<35°$N/S) (paleo)altimetry where T and RH over the oceans vary over quite limited ranges. Monthly mean T and RH data were extracted over entirely oceanic areas of the low latitude ($<35°$) part of the Earth from the 40 year

NCEP-CDAS reanalysis output [31]. Frequencies of corresponding T and RH values on a monthly basis were computed and used to determine the probability distribution functions from this data. We then employ simulation techniques to estimate the uncertainty of model-derived paleoaltitudes resulting from uncertainties in T and RH. Fig. 2 plots these results. Note that in this treatment we make predictions only about relatively low latitudes ($\leq$35°) and on long-term means. At higher latitudes the range of variability of T and RH is much larger, and storm trajectories and fronts are more complex. This is reflected, for example, in limited data from the Saint Elias Mountains [32] for a single storm event. We do not make predictions about individual precipitation events where variability can be much greater [20]. The model, as presented, does not explicitly take into account the role of isotopic readjustment associated with evaporation and exchange as the precipitation falls or effects of turbulent mixing. The largest effects are expected in areas where precipitation at high altitudes falls into significantly undersaturated air and evaporative re-enrichment of the precipitation occurs. The model takes some account of this in that the empirical fit derived from the Alps may incorporate some effects associated with exchange and evaporation and turbulent mixing.

4. Data–model comparison

The IAEA–GNIP data, as summarized by [20,33], reports isotopic compositions of precipitation for a number of high and low altitude, low latitude ($<35°$) stations that can be reasonably paired in order to estimate $\Delta(\delta^{18}O_p)$ (Fig. 3). Fig. 4 plots the results of a comparison of model $\Delta(\delta^{18}O_p)$ versus station elevations together with estimates of elevation uncertainty resulting from variance in T and RH. Fig. 4 shows station elevation versus predicted elevations derived from our model. The points that fall farthest from the

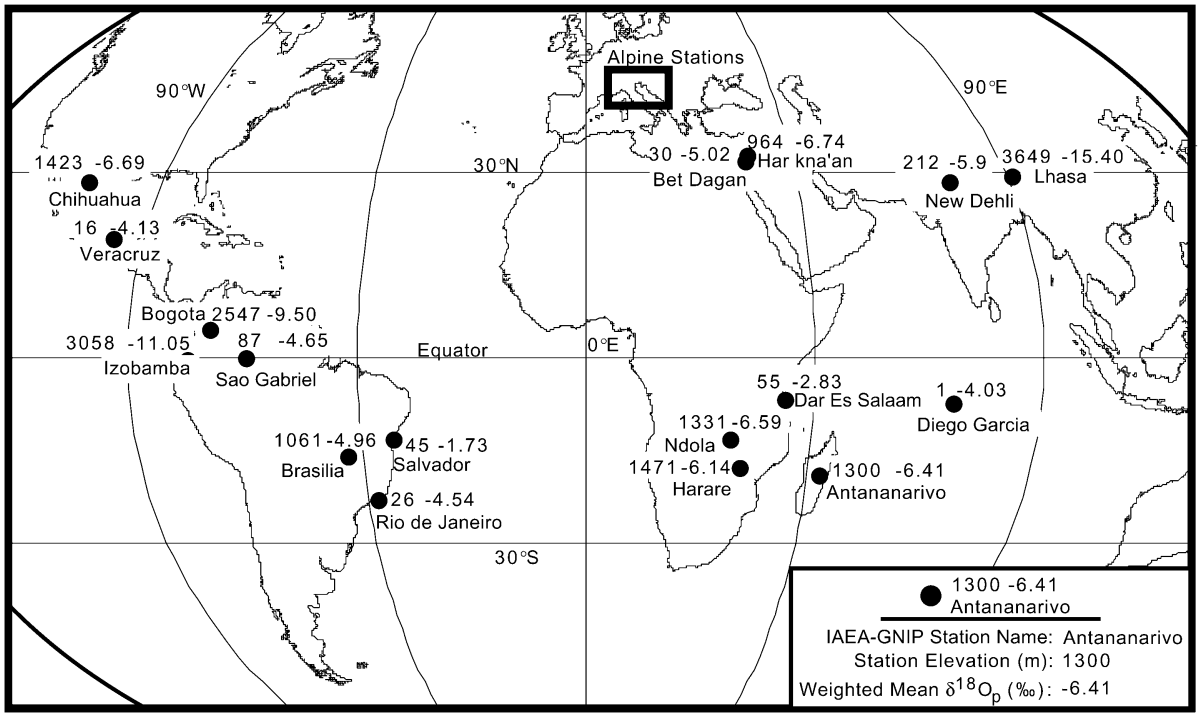

Fig. 3. Distribution of low latitude stations used to compute $\Delta(\delta^{18}O_p)$ with the heights and weighted mean compositions of the precipitation.

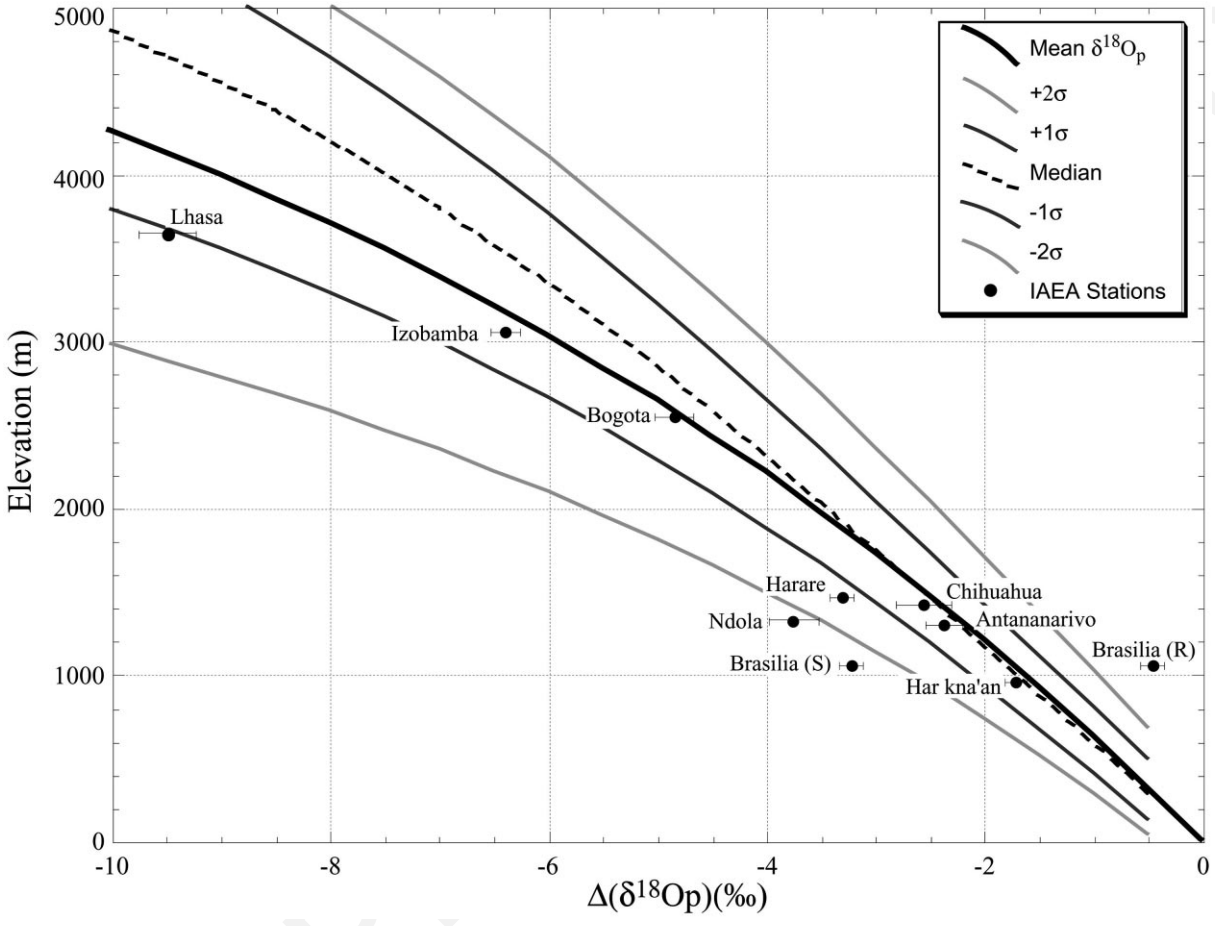

Fig. 4. $\Delta(\delta^{18}O_p)$ versus elevation of IAEA–GNIP stations versus trajectories of the predicted isotopic composition of precipitation.

curves in Figs. 4 and 5, including Brasilia, Ndola, and Harare, reflect contributions from several sources, including: (1) the sparseness of appropriate coastal stations upwind along the vapor trajectories resulting in an overestimate of $\Delta(\delta^{18}O_p)$, (2) all three stations are separated from low elevation stations by 1000 to 1500 km and hence subject to effects of continentality [20] that also results in an overestimate of $\Delta(\delta^{18}O_p)$, and (3) evidence that either the low altitude reference sites

Table 1
Estimates of the uncertainty in elevation based on $\Delta(\delta^{18}O_p)$

$\Delta(\delta^{18}O_p)$	Elevation (m)	Elevation uncertainty (+2σ)	Elevation uncertainty (+1σ)	Elevation uncertainty (−1 σ)	Elevation uncertainty (−2 σ)
−1.6	1000	463	201	249	417
−3.6	2000	716	381	313	657
−5.9	3000	1064	724	366	925
−9.0	4000	1405	1102	440	1209
−13.2	5000	1685	1381	555	1486
−19.5	6000	1833	1452	771	1749

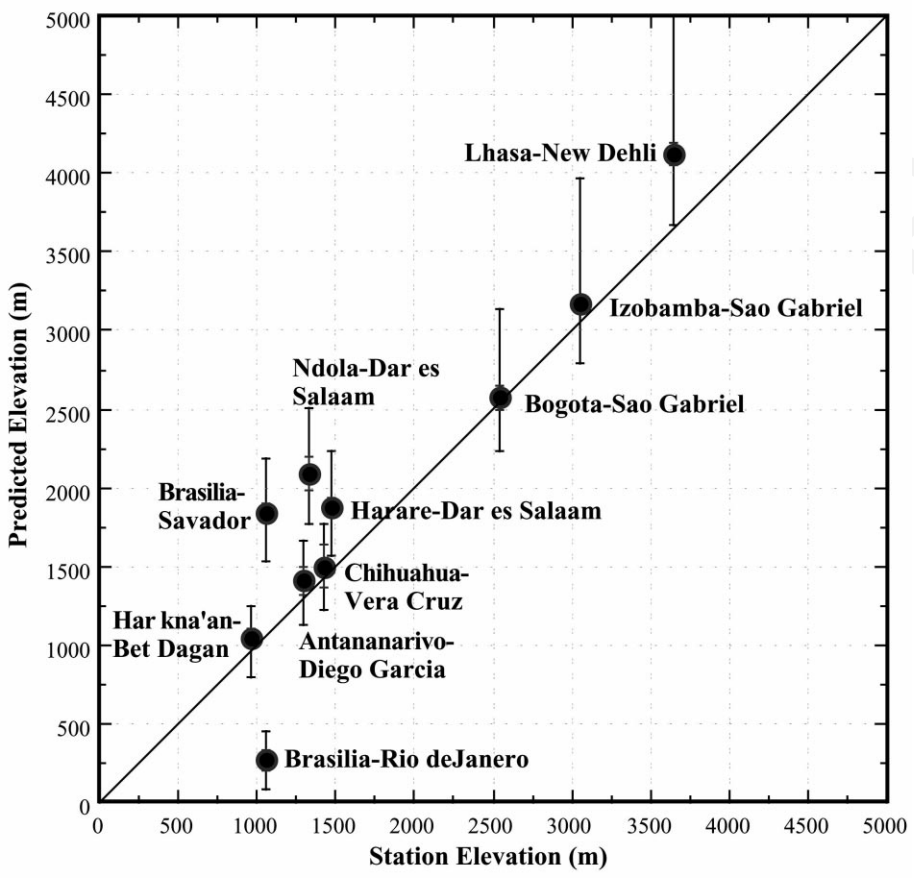

Fig. 5. IAEA–GNIP stations elevation versus predicted elevations for station pairs shown in Fig. 3.

and/or high altitude sites show significant scatter relative to the meteoric water line [33] reflecting rather well the effect of evaporative re-enrichment during fall into undersaturated air. Two sets of uncertainties are shown in Fig. 5. The smaller uncertainties reflect the combined standard errors of the means of the isotopic compositions of the low and high altitude stations as in Fig. 5, whereas the larger reflect the 1σ uncertainties in elevation as function of $\Delta(\delta^{18}O_p)$.

We derive estimates of the uncertainty of our results using simulations. The uncertainty reflects the range of starting T and RH of the air parcels. The distribution of elevations as a function of $\Delta(\delta^{18}O_p)$ are non-normal and asymmetric, and the results portrayed in Fig. 4 and tabulated in Table 1 are deviations calculated from frequency distributions of elevations versus $\Delta(\delta^{18}O_p)$ of the simulations expressed relative to the mean elevation. These estimates do not vary among simulations of 1000 to 5000 iterations.

This comparison suggests that the model captures the major features of the relationship of altitude and isotopic composition, and that the estimate of uncertainty is conservative.

5. Application to the Himalayas

The Tibetan Plateau is the largest region of high topography on Earth. The geodynamic evolution of Tibet is of considerable interest due to its enormous size ($> 5\,000\,000$ km^2), high average elevation (5023 m) [34,35], association with the Himalayan collisional orogen [36,37], and inferred influence on both regional and global climates [6–

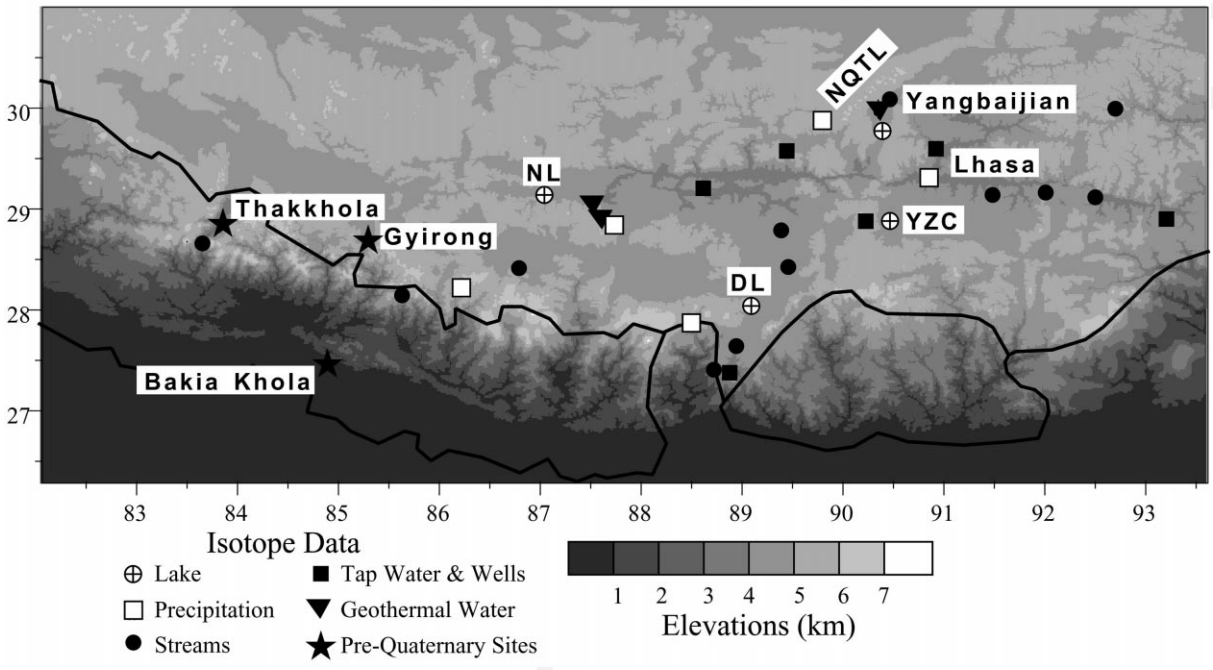

Fig. 6. Localities of modern and pre-Quaternary samples for oxygen isotope analysis superimposed on the topography of southern Tibet and Himalayas based on Globe (v.1) data. Sources listed in text. Abbreviations: DL, Doqen lake; NL, Namring Lake; NQTL, Nianqentangula Range; YZC, Yamzho Co.

10], ocean chemistry [38–42] and potentially CO_2 content of the atmosphere [43]. This high topography is isostatically supported by continental crust that is approximately 70 km thick, double the normal thickness [36]. A diverse array of geodynamic models invoking various mechanisms has been proposed to account for uplift and concomitant crustal thickening of Tibet and Himalayas. In virtually all models predictions are made regarding the initial timing, rate, duration, and spatial distribution of crustal thickening [44]. Although numerous geological and geophysical arguments have been made regarding the validity of the various models [37,44–46], the available data fail to provide unequivocal evidence for the surface uplift history of the region. Various qualitative estimates of the paleoaltitude of parts of the Himalayas and Tibet have made (e.g. [47]). There are serious questions regarding these estimates related to potential confounding of climate change and elevation change signals [48]. Thus current data are inadequate to estimate quantitatively paleoaltitudes useable in the assessment of the history of crustal and lithospheric thickening and mantle dynamics through time [44].

6. Present day Himalayan isotopic data–model comparison

Above we compared station elevation versus predicted elevations for a number of low latitude stations including Lhasa–New Delhi using the long-term IAEA–GNIP data [33]. Modern annual means were derived from weighted monthly means for New Delhi (elevation 212 m; $\delta^{18}O_p = -5.8 \pm 1.8‰$) [33] and Lhasa (3649 m; $\delta^{18}O_p = -15.4 \pm 1.5‰$ from data reported by IAEA through 1995 as released in 1997). New Delhi's isotopic composition is not different from the isotopic compositions of groundwater reported from the region extending as much as 1100 km eastward from New Delhi across India toward the Bay of Bengal [49]. We use the isotopic composition of New Delhi as our low altitude reference site and hence plot $\Delta(\delta^{18}O_p)$ rela-

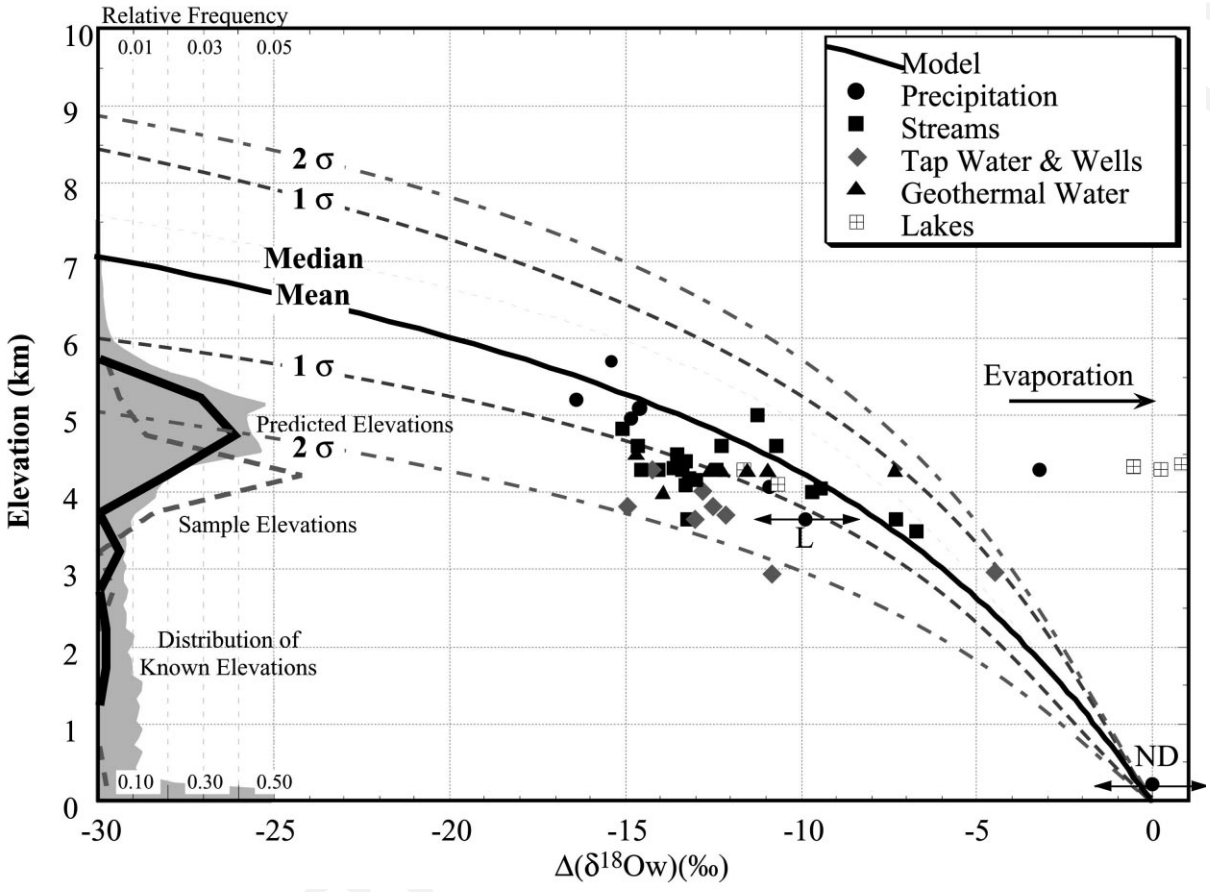

Fig. 7. Modern oxygen isotopic data from the Himalayas and southern Tibet versus elevation compared with modeled $\Delta(\delta^{18}O_p)$ in which the weighted mean isotopic composition of New Delhi is used as our low altitude reference. Locations of data are shown on Fig. 5. Solid light gray: relative frequency distribution of area by elevation corresponding to the region of Fig. 5 above 150 m derived from Globe (v.1) data. The boundaries of the region are from 30.0°N to 26.3125°N and 82.0708°E to 93.5875°E, essentially corresponding to the region from which the isotopic data were derived. Dashed gray line: relative frequency distribution of sample elevations. Black line: hypsometric distribution of elevations predicted from $\Delta(\delta^{18}O_p)$ isotopic compositions of water samples. Abbreviations: L, Lhasa; ND, New Delhi.

tive to this composition. Unfortunately additional long-term data are not available from the Himalaya–southern Tibet region. As a result we compare model results with published compositions of a variety of different hydrologic samples mostly collected as grab samples at discrete times (Figs. 6 and 7). In addition to the IAEA–GNIP data and those reported by Yu et al. [50] we also include data from modern snow from the Xixibangma and Changme Khangpu glaciers in the eastern Himalayas collected at elevations ranging from 4900 to 6100 m [51,52]. These data have a minimum value of about −21‰. The isotopic composition of the Kali Gandaki River is reported by Garzione et al. [53] to be −19.5 and −18.2‰ at elevations from 3300 to 3000 m. Finally we include the isotopic compositions of recent land snail shells collected from a terrace about 50 m above the Kali Gandaki River at about 3000 m and analyzed at the University of Chicago. The most depleted carbonate in these shells has a $\delta^{18}O_{c(PDB)}$ of −10.4‰. This composition corresponds with $\delta^{18}O_{p(SMOW)}$ of −11.3‰ at about 285 K appropriate for 3000 m elevation. Super-

imposed above these data in Fig. 7 are model estimates of the isotopic compositions of precipitation and estimates of $\pm 1\sigma$ and $\pm 2\sigma$ uncertainty in elevation corresponding to $\Delta(\delta^{18}O_p)$.

Comparison of existing measured compositions and model predictions are remarkably congruent. As expected, the observed compositions mostly fall along or below model compositions reflecting the fact that streams, tap water, wells, lakes, and geothermal waters all derive their precipitation from higher elevations than where they are sampled. The relative distribution of area within the eastern Himalayas and southernmost Tibet above 150 m (Fig. 7) demonstrates that a significant fraction lies above 5000 m and represents the source of the more depleted waters reflected in the Kali Gandaki and other sites shown on Fig. 6.

Three samples from lakes in the Himalayas, specifically from Yamzho Co, Doqen Lake, and Namgring Lake (Fig. 6) that range from -6.4 to $-5.1‰$ based on the limited sampling of Yu et al. [50], corresponding to $\Delta(\delta^{18}O_p) = -0.6$ to $0.7‰$ are clearly not accounted for within the context of the above model (Fig. 6). Two other lakes, Rawu and a lake in the Yangbaijain graben have compositions of $-16.6‰$ and $-17.5‰$ [50], respectively, are comparable with other hydrologic sources. Yamzho Co, Doqen Lake, and Namgring Lake are so-called terminal lakes in which evaporation is a significant contributor to the hydrologic balance. It is well understood that such lakes are characterized by potentially significant evaporative enrichment (arrow in Fig. 7) relative to input [54,55]. The compositions of these terminal lakes caution against over interpretation of less depleted isotopic compositions. We know of no process that results in enhanced isotopic depletion during orographic ascent after condensation of the precipitation and hence no process that would yield anomalously depleted compositions and falsely imply high elevation precipitation.

One approach to the interpretation of the modern $\Delta(\delta^{18}O_p)$ data is to simply focus on the most depleted values as these are likely the least affected by evaporation. However, if we assume that the variability of the existing modern data represents a random sample of elevations upon which the precipitation fell then this variability (excluding samples obviously impacted by evaporative enrichment) can be used to compute a predicted hypsometric distribution of elevations. Fig. 7 shows the comparison of the predicted hypsometry with the observed hypsometry showing clearly that the model yields a fairly accurate picture of the range of elevations within the sampled region (Fig. 7 – black curve at left) and thus serves as an additional independent test of our ability to use isotopes to predict elevations.

7. Paleoaltimetry of the High Himalayas

The primary purpose in developing this model is to provide a quantitative assessment of paleoelevations. The history of orogenesis (sensu stricto) in most mountain ranges is a matter of debate because virtually no direct quantitative data exist. One region, Himalayas–Tibet, has become the focus of particular attention due to its potential role in a wide range of long-term global change processes and the direct relevance of timing of uplift to tectonic models of continent–continent collisions. Existing indirect proxies for surface uplift [48] have been diversely interpreted as indicating significant topography predating collision [56,57] to surface uplift from about 1 km mean elevation to 5 km in the past 2–3 million years [58]. Can stable isotopic data from the High Himalayas help assess these various interpretations?

At present we have estimates of $\Delta(\delta^{18}O_p)$ from two Late Miocene and younger sequences within the High Himalayas. One sequence includes data from Late Miocene to late Pliocene lacustrine carbonates and calcareous fossils in the Gyirong Basin [59] (Fig. 5). This sequence has been dated magnetostratigraphically by Wang et al. [59] and includes reversals correlated with lower Matuyama ($\sim$1.7 Ma) to epoch 7 ($\sim$Chron 4, $\sim$7.4 to 8.1 Ma [60]). The isotopic composition of the carbonates from the Gyirong Basin range from $\delta^{18}O_{C(PDB)}$ of $-21.5‰$ to $-10.9‰$. The isotopic composition of water in equilibrium with these carbonates range from $\delta^{18}O_w$ of $-24.9‰$ to $-14.4‰$ at 275 K with a temperature related uncertainty of about $2‰$. Fig. 8 emphasizes a

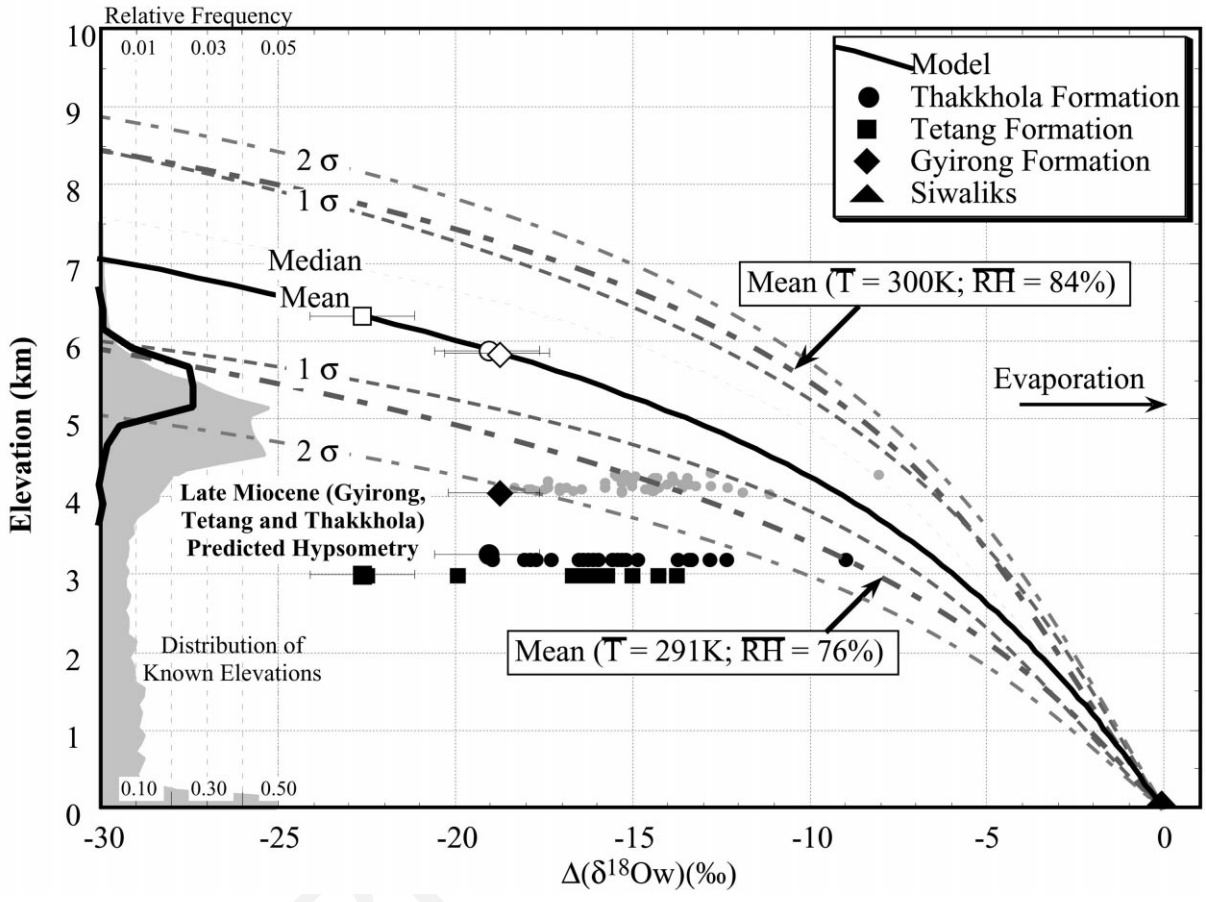

Fig. 8. Present elevations versus $\Delta(\delta^{18}O_p)$ of pre-Quaternary data from High Himalayan intermontaine basins. Data from Gyirong and Thakkhola and relatively more enriched values of the Tetang are from published sources [17,59], and for the Tetang from our data. The gray symbols plotted with the Gyirong data show the full range of data reported [59]. We use the average $\delta^{18}O_{p(SMOW)}$ derived from soil carbonates in the Siwaliks of Bakia Khola from [61] as our low altitude reference estimate. Open symbols represent the paleoaltitudes corresponding to the most negative values for each unit. Conversion of $\delta^{18}O_{Cc(PDB)}$ to $\delta^{18}O_{p(SMOW)}$ is based on equilibrium, temperature-dependent fractionation between carbonate and water [72] where temperatures and 1σ deviations of T derived from the model at the current elevation of each sample is used. Curves of mean T and RH at 300 K and 84%, and 291 K and 76% indicate corresponding changes in predicted elevation versus $\Delta(\delta^{18}O_p)$ if low latitude climate changes from present values by $\pm 1\sigma$ deviations of T and RH.

representative example of the data with corresponding uncertainties. The full range of the data are included without uncertainties. The second sequence is from the Thakkhola graben in Nepal [13,17]. These include data from soil carbonates, shells, and lacustrine micrites of the Thakkhola Formation [17], and lacustrine micrites reported by Garzione et al. [17] for the unconformably underlying Tetang Formation. In addition, we include our own measurements of ostracode-bearing carbonates from the basal part of the Late Miocene Tetang Formation (Fig. 6). The dating of the Tetang and Thakkhola Formations remains uncertain, but the current best estimate is that the base is of Late Miocene ($\sim$10 Ma) age [17]. The $\delta^{18}O_{C(PDB)}$ isotopic composition of carbonates from the Thakkhola range from −12.5‰ to −22.4‰ and Tetang range from −17.2‰ to about −23.4‰ according to Garzione et al. [17]. The $\delta^{18}O_w$ in equilibrium with these carbonates would range from about −13.7‰ to −24.6‰ at 284 K. Replicate mea-

surements of ostacode-bearing lacustrine carbonates of the lower Tetang Formation measured at the University of Chicago yield an isotopic composition of $-26‰ \pm 0.2‰$. These lower Tetang data are compatible with an isotopic composition of water in equilibrium with carbonates of $\delta^{18}O_{(SMOW)} = -27.2‰$ at 284 K to $-28.6‰$ at 278 K. In order to obtain $\Delta(\delta^{18}O_p)$, for the Tetang, Thakkhola, and Gyirong sequences, we use data from the Siwaliks of Bakiya Khola and Surai Khola, Nepal reported by Harrison et al. [61] and Quade et al. [62] (Fig. 5). The mean composition of these Late Miocene to Pliocene soil carbonates is $\delta^{18}O_{C(PDB)} = -8.6 \pm 2.6‰$. The precipitation at low elevations producing the soil water from which these carbonate nodules precipitated would be in equilibrium with a composition $\delta^{18}O_{(SMOW)} = -6.1 \pm 2.6‰$, essentially identical to modern low elevation precipitation at New Delhi. $\Delta(\delta^{18}O_p)$, as plotted in Fig. 8, is thus computed as the difference between Bakiya Khola and the various samples for Gyirong and Thakkhola basins.

One estimate of the paleoaltimetry of the regions from which Gyirong and Thakkhola basins derived their precipitation is provided by the most negative values of $\Delta(\delta^{18}O_p)$. These range from $\Delta(\delta^{18}O_p) \approx -22‰$ for the Tetang, $-18‰$ for the Thakkhola, and $-19‰$ from the Gyirong sequence. The corresponding estimates of the paleoaltitudes and 1σ uncertainties are 6240 m (+1410 m/−870 m) for the Tetang, 5700 m (+1410 m/−730 m) for the Thakkhola, and 5850 m (+1410 m/−730 m) Gyirong. These are shown on Fig. 8 by the open symbols plotted along the mean curve. Also plotted are the curves that reflect a change in the low latitude mean T and RH by $\pm 1\sigma$ in each of these parameters relative to the present. By most estimates global temperatures have decreased since the Late Miocene and hence the above represent perhaps underestimates of their corresponding paleoaltitudes.

In order to reasonably interpret the variability reflected in the data it is important to note three alternative interpretations. Wang et al. [59] interpreted the spread in the Gyirong sequence as reflecting climatic fluctuations in temperature; however, this is not viable as temperatures would have to vary by more than 45°C in order to yield this degree of variability from a constant composition source. Another interpretation is that since all of the samples are from lacustrine and or soil carbonate sequences, they probably record varying degrees of enrichment due to evaporation (Fig. 8 – arrow). The magnitude of the effect is dependent upon the degree of evaporation, and it could be argued that the more enriched values reported by both Garzione et al. [17] and Wang et al. [59] reflect evaporation. Alternatively, the spread in data may reflect a mixing relation between precipitation at and above the sampled locations. Such mixing might, for example, reflect seasonal differences in the mean elevation at which precipitation falls, or, in the case of snow, a seasonal change from accumulation versus melting. The fact that most of the points lie to the left and below the mean curve of expected compositions is certainly compatible with this last alternative. Theoretically various measures of evaporation, such as corresponding D/H ratios and deviations from the Meteoric Water Line, or through the correlation of $\Delta(\delta^{18}O_p)$ and Mg/Ca or Sr/Ca ratios of the carbonates could be used to determine the role of evaporation in controlling the isotopic variability of such samples. At present, data are not available from these sequences and hence we can not independently assess the degree to which evaporation may control isotopic compositions. If it is assumed that the third alternative is correct, and hence that this variability reflects a random sampling of the elevations upon which precipitation fell, then it is possible to estimate the paleohypsometry of the Himalayas in the vicinity of Gyirong and Thakkhola basins. The black curve to the left on Fig. 8 shows that the paleohypsometry is not significantly different from the present. Irrespective of the source of variability in these data, the isotopic compositions of Late Miocene to Plio–Pleistocene lacustrine carbonates preserved within the present High Himalayas imply that this region had already achieved elevations comparable to the present by about 10 Ma ago [13,53].

8. Summary

The quantitative estimate of paleoaltitude has become an increasing focus of Earth scientists as the importance of discerning paleoelevations has sharpened. The recent books [63] and [64] emphasize the importance of reconstructing paleoaltimetry. Chase et al. [11] in their review of existing paleoaltimeters note the potential of stable isotopes but comment that a coherent theory behind these estimates does not exist. Drummond et al. [15] have, in fact, inferred high paleotopography based on unusual oxygen isotopic compositions of Miocene Camp Davis lacustrine limestones, but assume a simple linear relationship between altitude and isotopic composition as have others [16,53].

Two other quantitative approaches to paleoaltimetry have been recently outlined and reviewed by Chase et al. [11] and Forest et al. [12]. These include use of foliar physiognomic approaches: (1) to use the difference in mean annual temperature estimates of a coastal and potential elevated inland site and an assumed lapse rate, or, (2) to use the difference in enthalpy between a coastal and potential elevated inland site at the same (paleo)latitude to estimate altitude. Both of these approaches derive from the correlation of various physiognomic characteristics of modern floras to modern climate parameters [12,65,66]. To apply these models to the past it is necessary to assume that precisely the same correlation exists for the paleo-floras, which is hard to assess quantitatively. Estimates of $\pm 1\sigma$ errors based on the differences in mean annual temperature are 660 m and 920 m at 2000 m and 4,00 m, respectively [12]. Estimates of $\pm 1\sigma$ errors based on the differences in enthalpy are between 620 and 910 m [12]. Finally, Sahagian and Maus [67] have suggested that the vesicularity of basalts correlates with atmospheric pressure. Their analysis suggests an altitude $\pm 1\sigma$ error of 0.1 bar or about 1–1.4 km. Estimated uncertainties are comparable among these methods but their applicability in the geologic past is quite variable. Both enthalpy and mean annual temperature differences require angiosperm floras. One would presume that the correlation of physiognomic characteristics to climate parameters will be increasingly influenced by evolutionary factors and hence that such estimates would become increasingly uncertain with geologic age. Irrespectively, these techniques are only applicable to the past 100 Ma or so. High altitude basalts, usually erupted as volcanoes above the mean surface have fairly limited preservation potential and hence limited applicability to the geologic past. By contrast, intermontaine basins are widely preserved in the geologic past and various sediments, including lacustrine carbonates, soil carbonates, fossil cellulose, fish teeth and otoliths and perhaps even select clays may retain records of fossil $\delta^{18}O_p$ or δD_p and hence provide the materials necessary for application of this model to virtually all times in the past.

Recent reviews of the evolution of Tibet and the Himalayas [10,35,37,44,45,68] emphasize the importance of topography as: (1) a monitor for collision dynamics [10]; (2) a measure of crustal mass balance [38,46,69,70]; (3) a significant influence on both the local and global climate [8,43,71]; and (4) a potential influence on both ocean [38,40] and atmospheric chemistry [39]. Existing interpretations of the evolution of the topography of Himalayas–Tibet range from suggestions of very large-scale uplift of much of Tibet in the last few million years [47,58] to recent suggestions that significant topography predated the initiation of the collision of India with Asia [56,57]. Stable isotope data from the High Himalayan intermontaine basins are not yet sufficient, either temporally or spatially, to provide a comprehensive assessment of the various models that have thus far been proposed. However, the data do imply that at least the High Himalayas had achieved their current hypsometry by the Late Miocene. Thus those models invoking significant increases in elevation in the last few million years [58,59] are clearly incompatible with these data. Better age control on the basal sequences of both the Gyirong basin and Tetang Formation is critical if we are to determine whether significant uplift of the Himalayas and Tibet occurred at about 8 Ma that might have been responsible for initiation or at least significant enhancement of the Asian monsoon [10,44].

Acknowledgements

This work greatly benefited from samples generously provided by Kip Hodges, Jose Hurtado, and Kelin Whipple from the Thakkhola basin in Nepal and to Bob Clayton and Tosh Mayeda for assistance and access to the stable isotope facilities at Chicago. Numerous discussions with many people, particularly Mike Foote, greatly improved the final result. We thank Jan Veizer, and Kacey Lohmann and two anonymous reviewers for their helpful comments and careful reviews.*[RV]*

References

[1] G. Houseman, P. England, A lithospheric-thickening model for the Indo–Asian collision, in: A. Yin, T.M. Harrison (Eds.), The Teconic Evolution of Asia, Cambridge University Press, Cambridge, 1996, pp. 3–17.

[2] P. England, G. Housemann, Finite strain calculations of continental deformation 2. Comparison with the India–Asia collision zone, J. Geophys. Res. 91 (1986) 3664–3676.

[3] M. Gurnis, J.X. Mitrovica, J. Ritsema, H. Van Heist, Density and dynamics of the African Superplume: Constraints from the joint use of African topography and Cenozoic uplift rate, Geochem. Geophys. Geosyst. 1, 2000.

[4] J.X. Mitrovica, C. Beaumont, G.T. Jarvis, Tilting of continental interiors by the dynamical effects of subduction, Tectonics 8 (1989) 1079–1094.

[5] M. Gurnis, Depressed continental hypsometry behind oceanic trenches; a clue to subduction controls on sea-level change, Geology 21 (1993) 29–32.

[6] W.F. Ruddiman, J.E. Kutzbach, I.C. Prentice, Testing the climatic effects of orography and CO_2 with General Circulation and Biome Models, in: W.F. Ruddiman (Ed.), Tectonic Uplift and Climate Change, Plenum, New York, 1997, pp. 203–235.

[7] D. Rind, G. Russell, W.F. Ruddiman, The effects of uplift on Ocean-Atmosphere circulation, in: W.F. Ruddiman (Ed.), Tectonic Uplift and Climate Change, Plenum, New York, 1997, pp. 123–147.

[8] J.E. Kutzbach, W.L. Prell, W.F. Ruddiman, Sensitivity of Eurasian climate to surface uplift of the Tibetan Plateau, J. Geol. 101 (1993) 177–190.

[9] J.E. Kutzbach, W.F. Ruddiman, W.L. Prell, Possible effects of Cenozoic uplift and CO_2 lowering on Global and Regional Hydrology, in: W.F. Ruddiman (Ed.), Tectonic Uplift and Climate Change, Plenum, New York, 1997, pp. 149–170.

[10] P. Molnar, P. England, J. Martinod, Mantle dynamics, uplift of the Tibetan Plateau, and the Indian Monsoon, Rev. Geophys. 31 (1993) 357–396.

[11] C.G. Chase, K.M. Gregory-Wodzicki, J.T. Parrish, P.G. DeCelles, Topographic history of the western Cordillera of North America and controls on climate, in: T.J. Crowley, K.C. Burke (Eds.), Tectonic Boundary Conditions for Climate Reconstruction, Oxford University Press, New York, 1998, pp. 73–97.

[12] C. Forest, J.A. Wolfe, P. Molnar, K.A. Emanuel, Paleoaltimetry incorporating atmospheric physics and botanical estimates of paleoclimate, Bull. Geol. Soc. Am. 111 (1999) 497–511.

[13] D.B. Rowley, R.T. Pierrehumbert, B.S. Currie, A. Hosman, R.N. Clayton, J. Hurtado, K. Whipple, K. Hodges, Stable isotope-based paleoaltimetry and the elevation history of the High himalaya since the late Miocene, Geological Society of America Abstracts with Program, 1999.

[14] R.T. Pierrehumbert, Huascaran delta O-18 as an indicator of tropical climate during the Last Glacial Maximum, Geophys. Res. Lett. 26 (1999) 1345–1348.

[15] C.N. Drummond, B.H. Wilkinson, K.C. Lohmann, G.R. Smith, Effect of regional topography and hydrology on the lacustrine isotopic record of Miocene paleoclimate in the Rocky Mountains, Paleogeogr. Paleoclimatol. Paleoecol. 101 (1993) 67–79.

[16] C.P. Chamberlain, M.A. Poage, Reconstructing the paleotopography of mountain belts from the isotopic composition of authigenic minerals, Geology 28 (2000) 115–118.

[17] C.N. Garzione, D.L. Dettman, J. Quade, P.G. DeCelles, R.F. Butler, High times on the Tibetan Plateau: Paleoelevation of the Thakkhola graben, Nepal, Geology 28 (2000) 339–342.

[18] W. Dansgaard, Stable isotopes in precipitation, Tellus 16 (1964) 436–468.

[19] W. Ambach, W. Dansgaard, H. Eisner, J. Mooler, The altitude effect on the isotopic composition of precipitation and glacier ice in the Alps, Tellus 20 (1968) 595–600.

[20] K. Rozanski, L. Araguas-Araguas, R. Gonfianti, Isotopic patterns in modern global precipitation, in: Climate Change in Continental Isotopic Records, Geophysical Monograph 78, American Geophysical Union, Washington, DC, 1993, pp. 1–36.

[21] J.R. Gat, The isotopes of hydrogen and oxygen in precipitation, in: P. Fritz, J.C. Fontes (Eds.), Handbook of Environmental Isotope Geochemistry, 1, Elsevier, Amsterdam, 1980, pp. 21–47.

[22] H. Craig, Isotopic variations in meteoric waters, Science 133 (1961) 1702–1708.

[23] C. Sonntag, K.O. Münnich, H. Jacob, K. Rozanski, Variations of Deuterium and Oxygen-18 in continental precipitation and groundwater, and their causes, in: A. Street-Perrott, et al. (Eds.), Variations in the Global Water Budget, D. Reidel, Amsterdam, 1983, pp. 107–124.

[24] J. Joussaume, R. Sadourny, J. Jouzel, A general circulation model of water isotopes in the atmosphere, Nature 311 (1984) 24–29.

[25] J. Jouzel, G. Russell, R. Suozzo, R. Koster, J. White, W.

Broecker, Simulations of the HDO and $^{1}H_{2}^{18}O$ atmospheric cycles using the NASA GISS general circulation model the seasonal cycle for present day conditions, J. Geophys. Res. 92 (1987) 11749–11757.
[26] L. Stowas, J.C. Moyano, Simulation of the isotopic content of precipitation, Atmos. Environ. 27A (1993) 327–333.
[27] S.D. Gedzelman, R. Arnold, Modeling the isotopic composition of precipitation, J. Geophys. Res. 99 (1994) 10455–10471.
[28] J. Horita, D.J. Wesolowski, Liquid–vapor fractionation of oxygen and hydrogen isotoopes of water from freezing to the critical temperature, Geochim. Cosmochim. Acta 58 (1994) 3425–3437.
[29] M. Majzoube, Fractionement en oxygen 18 et en deuterium entre l'eau et sa vapeur, J. Chem. Phys. 10 (1971) 1423–1436.
[30] L. Merlivat, G. Nief, Isotopic fractionation of solid–vapor and liquid–vapor changes of state of water at temperatures below 0°C, Tellus 19 (1967) 122–127.
[31] E. Kalnay, M. Kanamitsu, R. Kistler, W. Collins, D. Deaven, L. Gandin, M. Iredell, S. Saha, G. White, J. Woollen, Y. Zhu, M. Chelliah, W. Ebisuzaki, W. Higgins, J. Janowiak, K. Mo, C. Ropelewski, J. Wang, A. Leetmaa, R. Reynolds, R. Jenne, D. Joseph, The NCEP/NCAR 40-year reanalysis project, Bull. Am. Meteorol. Soc. 77 (1996) 437–471.
[32] G. Holdsworth, S. Fogarasi, H.R. Krouse, Variation of the stable isotopes of water with altitude in the Saint Elias Mountains of Canada, J. Geophys. Res. 96 (1991) 7483–7494.
[33] IAEA, Statistical Treatment of Data on Environmental Isotopes in Precipitation, International Atomic Energy Agency, Vienna, 1992, 781 pp.
[34] E.J. Fielding, B.L. Isacks, M. Barazangi, C.C. Duncan, How flat is Tibet? Geology, 1996.
[35] E.J. Fielding, Tibet uplift and erosion, Tectonophysics 260 (1996) 55–84.
[36] E. Argand, La Tectonique de L'Asie, in: Proc. XIIIth Int. Geol. Congr. 1, pt 5, Brussels, 1924, pp. 181–372.
[37] J.F. Dewey, R. Shackleton, C.F. Chang, Y.Y. Sun, The tectonic evolution of Tibet, in: The Geological Evolution of Tibet, The Royal Society, London, 1988, pp. 379–413.
[38] F. Richter, D.B. Rowley, D.J. DePaolo, Sr isotope evolution of seawater the role of tectonics, Earth Planet. Sci. Lett. 109 (1992) 11–23.
[39] M.E. Raymo, Geochemical evidence supporting T.C. Chamberlin's theory of glaciation, Geology 19 (1991) 344–347.
[40] J. Edmonds, Himalayan tectonics, weathering processes, and the strontium isotope record in marine limestones, Science 258 (1992) 1594–1597.
[41] L.A. Derry, C. France-Lanord, Himalayan weathering and erosion fluxes: climate and tectonic controls, in: W.F. Ruddiman (Ed.), Tectonic Uplift and Climate Change, Plenum, New York, 1997, pp. 289–312.
[42] S.E. McCauley, D.J. DePaolo, The marine $^{87}Sr/^{86}Sr$ and $\delta^{18}O$ records, Himalayan alkalinity fluxes, and Cenozoic climate models, in: W.F. Ruddiman (Ed.), Tectonic Uplift and Climate Change, Plenum, New York, 1997, pp. 427–467.
[43] M.F. Raymo, W.F. Ruddiman, Tectonic forcing of late Cenozoic climate, Nature 359 (1992) 117–122.
[44] T.M. Harrison, P. Copeland, W.S.F. Kidd, Y. An, Raising Tibet, Science 255 (1992) 1663–1670.
[45] P. Copeland, The when and where of the growth of the Himalaya and the Tibetan Plateau, in: W.F. Ruddiman, (Ed.), Tectonic Uplift and Climate Change, Plenum, New York, 1997, pp. 19–40.
[46] J.F. Dewey, S.C. Cande, W.C. Pitman, Tectonic evolution of the India/Eurasia collision zone, Eclogae Geol. Helv. 82 (1989) 717–734.
[47] J.L. Mercier, R. Armijo, P. Tapponier, E. Carey-Gailhardis, T.L. Han, Change from late Tertiary compression to Quaternary extension in southern Tibet during the India–Asia collision, Tectonics 6 (1987) 275–304.
[48] P. England, P. Molnar, Surface uplift, uplift of rocks, and exhumation of rocks, 1990, 18, 1990, 1173–1177.
[49] R.V. Krisnamurthy, S.K. Bhattacharya, Stable oxygen and hydrogen isotope ratios in shallow ground waters from India and a study of the role of evapotranspiration in the Indian monsoon, in: H.P. Taylor, J.R. O'Neil, I.R. Kaplan,(Eds.), Stable Isotope Geochemistry: A tribute to Samuel Epstein, Spec. Publ. 3, pp. 187–203, Geochemical Society, San Antonio, TX, 1991.
[50] J. Yu, H. Zhang, F. Yu, D. Liu, Oxygen isotopic composition of meteoric water in the eastern part of Xizang, in: D. Liu, (Ed.), Geological and Ecological Studies of Qinghai–Xizang Plateau: Geology, Geological History and origin of Qinghai–Xizang Plateau, Science Press, Beijing, 1981, pp. 1677–1686.
[51] V. Aizen, E. Aizen, J. Melack, T. Martma, Isotopic measurements of precipitation on central Asian glaciers (southeastern Tibet, northern Himalayas, central Tien Shan), J. Geophys. Res. 101 (1996) 9185–9196.
[52] N. Bhandari, V.N. Nijampukar, C.P. Vohra, Radiometric chronology of some Himalayan Glaciers, in: A. Street-Perrott, et al. (Eds.), Variations in the Global Water Budget, D. Reideel, Amsterdam, 1983, pp. 207–216.
[53] C.N. Garzione, J. Quade, P.G. DeCelles, N.B. English, Predicting paleoelevation of Tibet and the Himalaya from $\delta^{18}O$ vs. altitude gradients in meteoric water across the Nepal Himalaya, Earth Planet. Sci. Lett. 183 (2000) 215–229.
[54] J.R. Gat, Oxygen and hydrogen isotopes in the hydrologic cycle, Annu. Rev. Earth Planet. Sci. 24 (1996) 225–262.
[55] H. Craig, L.I. Gordon, Deuterium and oxygen-18 variations in the ocean and marine atmosphere, in: E. Tongiorgi (Ed.), Stable Isotopes in Oceanographic studies and Paleo-Temperatures, Conferences in Nuclear Geology, Spoleto, Pisa, 1965, pp. 9–130.
[56] P. England, M.J. Searle, The Cretaceous–Tertiary deformation of Lhasa block and its implications for crustal thickening in Tibet, Tectonics 5 (1987) 1–14.

[57] M.A. Murphy, A. Yin, T.M. Harrison, S.B. Dürr, Z. Chen, F.J. Ryerson, W.S.F. Kidd, X. Wang, X. Zhou, Did the Indo–Asian collision alone create the Tibetan plateau?, Geology 25 (1997) 719–722.
[58] R. Xu, Vegetational changes in the past and the uplift of Qinghai–Xizang plateau, in: D.S. Liu, et al. (Eds.), Geological and Ecological Studies of Qinghai–Xizang Plateau I, Science Press, Beijing, 1981, pp. 139–148.
[59] F.B. Wang, S.F. Li, X.H. Shen, J. Zhang, G. Yan, Formation, evolution and environmental changes of the Gyirong Basin and uplift of the Himalaya, Sci. China Ser. D 39 (1996) 401–409.
[60] W.A. Berggren, D.V. Kent, C.C. Swisher, III, M.P. Aubry, A revised Cenozoic geochronology and chronostratigraphy, in: W.A. Berggren, D.V. Kent, M.P. Aubry, J. Hardenbohl (Eds.), Time Scales and Global Stratigraphic Correlation, Spec. Publ. 54, Society of Economic Paleontologists and Mineralogists, 1995, pp. 129–218.
[61] T.M. Harrison, P. Copeland, S. Hall, J. Quade, S. Burner, T.P. Ojha, W.S.F. Kidd, Isotope preservation of Himalayan/Tibetan uplift denudation and climatic histories of two molasse deposits, J. Geol. 101 (1993) 157–176.
[62] J. Quade, J.M.L. Cater, T.P. Ojha, J. Adam, T.M. Harrison, Late Miocene environmental change in Nepal and the northern Indian subcontinent: Stable isotopic evidence from paleosols, Geol. Soc. Am. Bull. 107 (1995) 1381–1397.
[63] W.F. Ruddiman, Tectonic Uplift and Climate Change, Plenum, New York, 1997, 535 pp.
[64] T.J. Crowley, K.C. Burke, Tectonic Boundary Conditions for Climate Reconstructions, Oxford University Press, Oxford, 1998, 285 pp.
[65] J.A. Wolfe, A method for obtaining climate parameters from leaf assemblages, US Geol. Surv. Bull. 1964, 1993, 35 pp.
[66] K.M. Gregory, Paleoclimate and paleoelevation of the 35 Ma Florissant flora, Front Range, Colorado, Paleoclimates 1 (1994) 23–57.
[67] D.L. Sahagian, J.E. Maus, Basalt vesicularity as a measure of atmospheric pressure and paleoelevation, Nature 372 (1994) 449–451.
[68] B.C. Burchfiel, L.H. Royden, Tectonics of Asia 50 years after the death of Emile Argand, Eclogae Geol. Helv. 84 (1991) 599–629.
[69] P. England, G. Housemann, Finite strain calculations of continental deformation. II: Application to the India–Asia plate collision, J. Geophys. Res. 91 (1986) 3664–3676.
[70] X. LePichon, M. Fournier, L. Jolivet, Kinematics, topography, shortening and extrusion in the India–Eurasia collision, Tectonics 11 (1992) 1085–1098.
[71] G. Ramstein, F. Fluteau, J. Besse, S. Joussaume, Effects of orogeny, plate motion and land–sea distribution on Eurasian climate change over the past 30 million years, Nature 386 (1997) 788–795.
[72] I. Friedman, J.R. O'Neil, Compilation of stable isotope fractionation factors of geochemical interest, in: M. Fleischer (Ed.), Data of Geochemistry, Professional Paper 440, US Geol. Surv., Washington, DC, 1977.